pling from gates A and B to the output dots added a monotonic term to the border shift, but its magnitude was smaller than that of the periodic shift over the voltage range of one electron switch in the input dots.

We compared the observed border shift with theoretical results (Fig. 3A), which include cancelation voltages and all experimentally determined capacitances. The theoretical results were obtained by minimizing the classical electrostatic energy for the array of islands and voltage leads. The full-capacitance matrix was included, and the minimum energy charge configuration was calculated subject to the condition that island charge be an integer multiple of electronic charge. Finite temperature effects were obtained by thermodynamic averaging over all nearby charge configurations. Experiment and theory match very well with only the substrate background charge and temperature as fitting parameters. The background charge adds a random offset to the position of the border but does not change the magnitude or period of the observed shift. The best fit to experiment is obtained for a temperature of 50 mK. The discrepancy between this and the base temperature of the dilution refrigerator (15 mK) most likely occurs because of heating of the electron subsystem by electromagnetic and thermal noise sources (*7*) and the applied 4-μV excitation. This effect is common in transport experiments at temperatures below 100 mK (*6*, *7*).

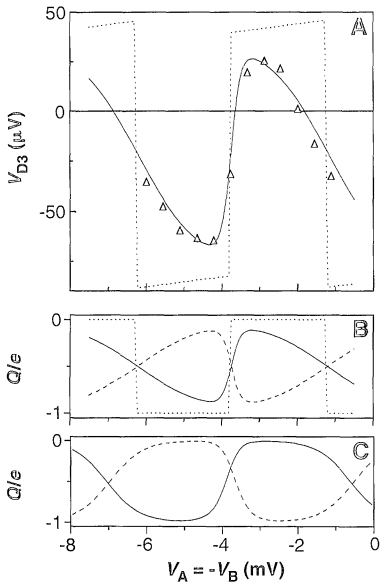

Fig. 4. (**A**) Voltage on dot D3 of output double dot as a function of driver voltage $V_A = -V_B$. Triangles are experimental data, and solid line represents theoretical values at 50 mK. For reference, theoretical data at 0 K (dotted line) are shown. (**B**) Calculated charge on dots D3 and D4 as a function of driver voltage for $C_{D1D2} = C_{D2D4} = 0.65$ *e*/mV (experimental value). Solid line represents charge on dot D3 at 50 mK, dashed line is charge on dot D4 at 50 mK, and dotted line is charge on D3 at 0 K. (**C**) Calculated charge on dots D3 and D4 as a function of driver voltage for $C_{D1D2} = C_{D2D4} = C_{junction} = 2.1$ *e*/mV. Solid line is charge on dot D3 at 50 mK, and dashed line is charge on dot D4 at 50 mK.

To show that the observed border shift represents a polarization switch of the cell at finite temperature, we combined the results of the border-shift measurements (Fig. 3) with measurements of the electrostatic potentials of the double dot. The electrostatic potential of each dot in the double dot was measured with the same device but with D1 and D2 as electrometers (*8*). The result is shown in Fig. 4A, where we plot electrostatic potential on dot D3 as measured by electrometer D1, together with theoretical calculations of the same potential at 0 and 50 mK, as a function of driver voltage V_A. The calculated excess charge on islands D3 and D4 of the double dot at 50 mK and, for reference, the charge on D3 at 0 K are indicated in Fig. 4B. Charge switching occurs at $V_A \sim -3.8$ mV, corresponding to an electron switch in the input dots. An input voltage swing $\Delta V_A = -\Delta V_B$ of 1.3 mV is sufficient for nearly complete transfer of an electron from one output dot to the other. An increase in coupling capacitance $C_{D1D3} = C_{D2D4}$ would lead to a more complete electron transfer, as shown in the theoretical plot (Fig. 4C), where we set the coupling capacitance to be equal to a junction capacitance. The data of Fig. 4 confirm that the experimentally observed honeycomb shift represents the polarization change of a functioning QCA cell.

The QCA architecture is a break from the FET-based paradigm of digital logic. Logic levels are encoded no longer as voltages on capacitors, which must be charged and discharged by current switches, but rather as the positions of electrons within a cell. The scalability of QCA offers the future possibility of functional devices that, at the molecular level, can operate at room temperature.

REFERENCES AND NOTES

1. C. S. Lent, P. D. Tougaw, W. Porod, G. H. Bernstein, *Nanotechnology* **4**, 49 (1993); C. S. Lent and P. D. Tougaw, *Proc. IEEE*, **85**, 541 (1997).
2. K. K. Likharev, *IBM J. Res. Dev.* (January 1988), p. 114.
3. P. D. Tougaw and C. S. Lent, *J. Appl. Phys.* **75**, 1818 (1994).
4. T. A. Fulton and G. H. Dolan, *Phys. Rev. Lett.* **58**, 109 (1987).
5. H. Pothier *et al.*, *Physica B* **169**, 573 (1991).
6. P. Lafarge *et al.*, *Z. Phys. B* **85**, 327 (1991).
7. D. Vion *et al.*, *J. Appl. Phys.* **77**, 2519 (1995).
8. I. Amlani, A. O. Orlov, G. L. Snider, G. H. Bernstein, unpublished results.

9. Supported in part by Defense Advanced Research Project Agency, Office of Naval Research (grant N00014-95-1-1166), and NSF. We thank W. Porod and J. Merz for useful discussions.

15 May 1997; accepted 23 June 1997

Structure, Bonding, and Geochemistry of Xenon at High Pressures

Wendel A. Caldwell, Jeffrey H. Nguyen, Bernd G. Pfrommer, Francesco Mauri, Steven G. Louie, Raymond Jeanloz

Although xenon becomes metallic at pressures above about 100 gigapascals, a combination of quantum mechanical calculations and high pressure–temperature experiments reveals no tendency on the part of xenon to form a metal alloy with iron or platinum to at least 100 to 150 gigapascals. The transformation of xenon from face-centered cubic (fcc) to hexagonal close-packed (hcp) structures is kinetically hindered, the differences in volume and bulk modulus between the two phases being smaller than we can resolve (less than 0.3 percent and 0.6 gigapascals, respectively). The equilibrium fcc-hcp phase boundary is at 21 (±3) gigapascals, which is a lower pressure than was previously thought, and it is unlikely that Earth's core serves as a reservoir for primordial xenon.

Like the other noble elements, Xe is characterized by a reluctance to form chemical bonds. Indeed, chemical inertness makes the noble gases useful as tracers that help reveal the evolution of planetary atmospheres and interiors (*1*–*6*). That Xe can bond to form compounds (*7*–*9*) and even, at high pressures, a hexagonal close-packed (hcp) metal (*10*–*12*), opens up the possibility that geochemical trends of the planets' noble gas abundances can be influenced by chemical reactions taking place at the elevated pressures and temperatures of planetary interiors. Specifically, the relative depletion of Earth's atmospheric Xe compared with meteoritic and solar abundances—the geochemical "missing Xe" problem (*2*, *13*, *14*)—suggests that significant amounts of Earth's primordial Xe could be sequestered at depth,

inside the core (*15*, *16*).

Here we investigate whether chemical interactions taking place at high pressures may influence the distribution of Xe within the planet. This is an extension of lower pressure studies that indicate no special tendency of Xe to bind with and partition into core-forming Fe up to pressures of 10 gigapascals(GPa) (*17*). However, the properties and even the equilibrium phase transitions of Xe at high pressures remain unclear. For example, Jephcoat *et al.* (*18*) found from x-ray diffraction studies at room temperature that Xe is stable in the face-centered cubic (fcc) phase up to 14 GPa and in the hcp phase above 75 GPa up to at least 137 GPa, but the diffraction pattern and crystal structure were not well resolved at intermediate pressures.

Using a laser-heated diamond-anvil cell we carried out experiments on samples of Xe and Fe up to pressures of 70 GPa (*19*). For a sample held at a pressure of about 50 GPa, the x-ray diffraction pattern changed as the sample was heated to peak temperatures of 3000 K (Fig. 1) (*20*). We believe that the change in diffraction pattern is due to the Xe transforming from fcc to hcp structures, without any indication of chemical reaction between the Fe and Xe, for two reasons. First, the diffraction pattern after heating at 50 GPa corresponds to that expected for a mixture of fcc and hcp Xe, along with unreacted hcp Fe. After accounting for the pressure dependence of lattice parameters and the presence of Fe, our 50-GPa diffraction pattern is identical to the diffraction patterns obtained by us and by Jephcoat *et al.* (*18*) for Xe taken to 70 to 75 GPa without heating. Chemical reactions are unlikely to occur in the unheated samples. Therefore, our interpretation for the 50-GPa samples after heating is that these are just like the unheated samples at 70 to 75 GPa: In both cases, Xe is simply in the process of undergoing a structural transformation that is kinetically sluggish but is aided by laser heating in the 50-GPa experiment. Second, we carried out independent experiments on samples of Pt and Xe laser-heated at 50 GPa. Platinum is expected to be less reactive than Fe, and we obtained identical results as before: The x-ray diffraction patterns can be entirely explained in terms of a combination of fcc and hcp phases of Xe, along with unreacted fcc Pt.

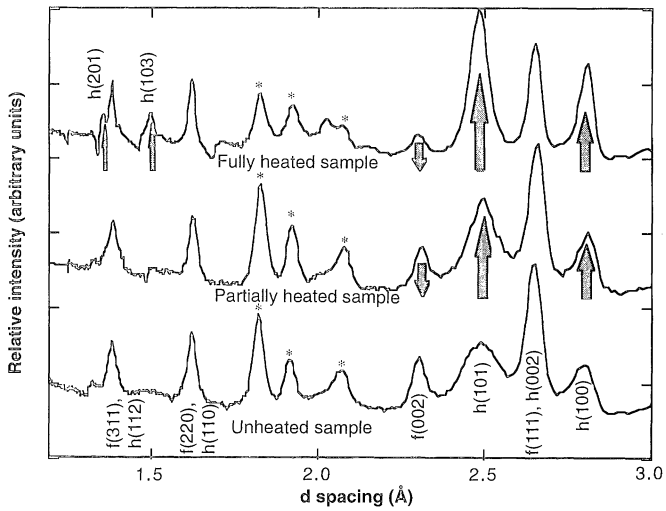

Fig. 1. Structural transformation of crystalline Xe shown by changes in x-ray diffraction patterns taken at high pressure but room temperature, before and after partial and then complete heating to peak temperatures of 3000 (±300) K at 53 (±2) to 47 (±2) GPa (pressure relaxes slightly upon heating) (f, fcc; h, hcp). Arrows indicate shifts in peak intensities due to growth of the hcp relative to the fcc phase of Xe with increased heating, and asterisks indicate peaks due to Fe in the sample. Two peaks in the unheated sample are identified as the (101) and (100) diffraction lines from hcp Xe. After the sample is heated, first partially then fully, the hcp (101) and (100) peaks grow in intensity while the fcc (200) peak diminishes in intensity. The diffraction pattern of the fully heated sample also shows evidence of new peaks that can be indexed as hcp (201) and (103) peaks.

The results for Pt + Xe samples confirm that the fcc → hcp transformation of Xe is kinetically sluggish and therefore goes toward completion at much lower pressures on laser heating than when the sample is merely compressed at room temperature. The crystallographic unit-cell parameters for the fcc and hcp structures are coherent over the broad pressure range in which the two phases are observed to coexist (Fig. 2). The fact that we can continuously and reversibly track the evolution of diffraction patterns, from fcc at low pressures to nearly pure hcp at higher pressures, gives us confidence that we are documenting a crystal structural transformation rather than a chemical reaction.

In order to further check this conclusion, we carried out ab initio total-energy calculations within the framework of density functional theory in the local density approximation (LDA) (*21*). Enthalpy calculations were performed to determine the stability of a set of Xe and Fe compounds—XeFe, Xe_2Fe, and $XeFe_2$—in hcp packing relative to that of separated Xe and Fe in their high-pressure hcp phases (Table 1). For high pressures (>100 GPa), we also considered the hexagonal Laves phase of $XeFe_2$, a structure that corresponds to an optimal packing of Fe and Xe atoms having different atomic radii (*22*). One way of checking the validity of the theoretical calculations is to compare them with the high-

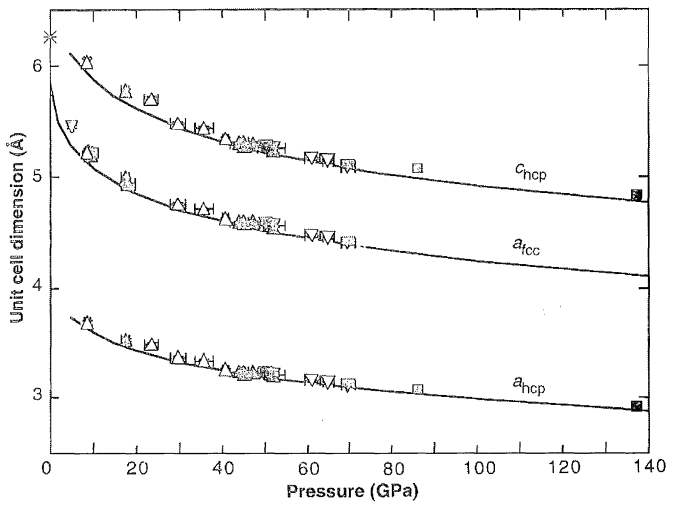

Fig. 2. Unit cell parameters for the fcc (*a*) and hcp (*a*,*c*) phases of Xe plotted against pressure. Lines are from our theoretical calculations for the static lattices, whereas symbols indicate experimental results from the present study (upward-pointing triangles, samples containing Xe and Fe; downward-pointing triangles, samples containing Xe and Pt; solid and open symbols indicate measurements taken upon compression and decompression, respectively); from the work of Jephcoat *et al.* (*18*) (squares); and from previous determinations of the fcc lattice parameter at zero pressure and 88 K (*30*) (asterisk at upper left). In our study, the lattice parameters were determined from (111), (220), and (311) and from (100), (002), (101), and (110) diffraction peaks for the fcc and hcp structures, respectively, and the uncertainties are smaller than the symbols.

W. A. Caldwell and R. Jeanloz, Department of Geology and Geophysics, University of California, Berkeley, CA 94720, USA.
J. H. Nguyen, Department of Physics, University of California, Berkeley, CA 94720, USA.
B. G. Pfrommer, F. Mauri, S. G. Louie, Department of Physics, University of California, Berkeley, CA 94720, USA, and Materials Sciences Division, Lawrence Berkeley National Laboratory, Berkeley, CA 94720, USA.

pressure x-ray diffraction measurements on the fcc and hcp phases of Xe. We find agreement between the calculated and observed lattice parameters of the two phases of Xe; the theoretical lattice parameters are slightly lower than the observed values, as is expected, because the former is for the static lattice (Figs. 2 and 3).

Over the pressure range 0 to 500 GPa, the Xe-Fe compounds are all energetically unfavorable (Table 1). Even at 500 GPa, the enthalpy of the most favorable compound that we considered, the Laves phase, exceeds that of separate Xe and Fe by a respectable 0.9 eV per formula unit. Indeed, theoretical diffraction patterns calculated for each of the four Xe-Fe phases listed in Table 1 yield no match with any of the experimental results.

More than just confirming the experimental findings, the theoretical calculations are important for understanding why the compounds are so energetically unstable. We find that although the Fe atoms form bonds among each other, the spherical charge distribution around the Xe sites remains relatively undistorted, showing the lack of any significant bonding with the Xe at high pressures. Thus, any incipient Xe-Fe bonding is so weak that it does not compensate for the energetic cost of breaking the strong Fe-Fe bond in iron, even at 150 to 500 GPa; the energetics are so unfavorable that this is likely to be true for other structures and Fe/Xe stoichiometries than those we have considered. In short, the theoretical calculations support our conclusion that the experiments solely document the transformation of Xe from fcc to hcp structures.

Systematic experiments with increasing and decreasing pressure provide an estimate of 18 to 24 GPa for the equilibrium fcc ↔ hcp transition pressure of Xe at room temperature and to ~2000 to 3000 K, but with a pressure range of 9 to 70 GPa, over which we observe the coexistence of both phases because of the sluggish kinetics (Figs. 2 and 3). Theoretically, we calculate that the phase transition is expected to occur at about 5 GPa for the static lattice, which is in general agreement with the experimental results. Our static-lattice calculations ignore vibrational (zero-point and thermal) effects and may suffer from the shortcomings of the LDA. Therefore, the agreement between theory and experiment may be somewhat fortuitous, yet the small energy difference calculated for the two phases is in accord with the experimentally observed sluggishness of the phase transition. The thermodynamic driving force for the fcc → hcp transition is small (*23*). McMahan (*24*) discusses the origin of this driving force for argon.

The similarity in energies between the fcc and hcp phases is highlighted by our finding that the two phases have experimentally indistinguishable pressure-volume equations of state (*25–27*). The close similarity between the fcc and hcp structures, which have identical first- and second-neighbor coordination shells, explains why the volumes of the two phases are difficult to distinguish (*23*, *28*). Along with the sluggishness of the transformation, the close orientation relation between the two structures (*26*) can explain why Jephcoat *et al.* (*18*) observed complex x-ray diffraction patterns from Xe compressed at room temperature (without heating) between 14 and 75 GPa.

Although the bonding in Xe, like the other noble gases, has often been modeled through the use of pair potentials, the relatively low fcc-hcp transition pressure illustrates a deviation from such a simple model for the interatomic forces at high pressures; the transition pressure is predicted to be about 64 GPa, even when three-body interaction terms are included (*29*). For comparison, the ab initio quantum mechanical approach presented here is in agreement with the experimental determinations of the transition pressure and equations of state of the two known crystalline phases of Xe.

In summary, theory and experiment argue against the likelihood of Xe bonding with Fe over the pressure range examined here, and hence of Xe having partitioned into core-forming metal to any significant degree inside Earth. It appears that the "missing Xe" problem of planetary geochemistry must be resolved by other mechanisms (*2*, *3*, *14*, *17*). In particular, the observed pattern of noble gas abundances appears to have been set before Earth and the terrestrial planets were fully accreted, rather than having been subsequently modified due to inclusion into the core.

Table 1. Formation enthalpies of XeFe compounds from theory* (electron volts per formula unit).

Pressure (GPa)	XeFe ($P\bar{6}m2$)	Xe_2Fe ($P\bar{3}m1$)	$XeFe_2$ ($P\bar{3}m1$)	$XeFe_2$ Laves phase ($P6_3/mmc$)
0	5.2	5.7	4.9	—
50	3.7	4.3	4.4	—
100	3.0	3.6	4.2	—
150	2.6	3.2	3.9	3.1
500	1.0	1.4	2.8	0.9

*The enthalpy of the compound (a crystal in a given space group) minus the enthalpy of the separate elements.

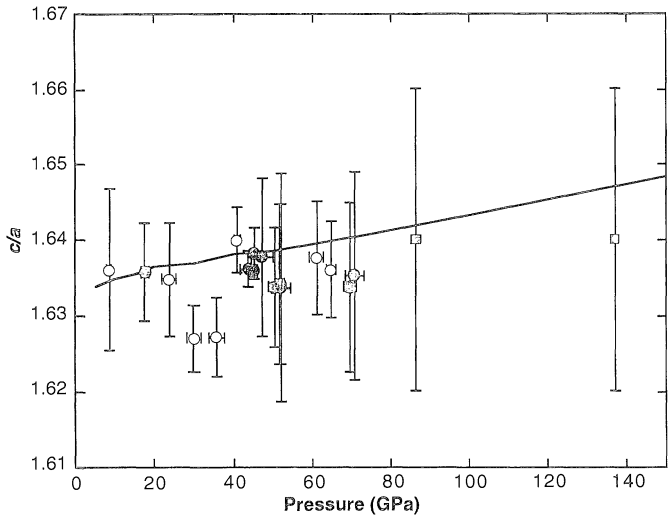

Fig. 3. Comparison of experimentally and theoretically determined ratios of Xe hcp unit cell parameters, *c/a*, plotted against pressure. Solid and open circles indicate measurements taken on compression and decompression, respectively, whereas the line indicates results from theory squares are from the work of Jephcoat *et al.* (*18*). Compatible with experimental results, the theoretical values are generally close to the ideal ratio for hcp packing of identical spheres, $\sqrt{8/3} = 1.633$, and rise slowly with increasing pressure.

REFERENCES AND NOTES

1. M. Ozima and F. A. Podosek, *Noble Gas Geochemistry* (Cambridge Univ. Press, New York, 1983).
2. C. J. Allegre, T. Staudacher, P. Sarda, *Earth Planet. Sci. Lett.* **81**, 127 (1986).
3. R. O. Pepin, *Icarus* **92**, 2 (1991); *Annu. Rev. Earth Planet. Sci.* **20**, 389 (1992).
4. M. Ozima, *Rev. Geophys.* **32**, 405 (1994).
5. D. Porcelli and G. J. Wasserburg, *Geochim. Cosmochim. Acta* **59**, 1991 (1995).
6. C. L. Harper Jr. and S. B. Jacobsen, *Science* **273**, 1814 (1996).
7. N. Bartlett, *Proc. Chem. Soc.* **1962**, 218 (1962).
8. L. C. Allen, *Ann. N.Y. Acad. Sci.* **118**, 883 (1965).
9. R. Steudel, *Chemistry of the Non-Metals* (Walter de Gruyter, New York, 1977), pp. 270–278.
10. K. A. Goettel, J. H. Eggert, I. F. Silvera, W. C. Moss, *Phys. Rev. Lett.* **62**, 665 (1989).
11. R. Reichlin *et al.*, *ibid.*, p. 669.
12. H. Chacham, X. Zhu, S. G. Louie, *Phys. Rev. B* **46**, 6688 (1992).
13. D. Krummenacher, C. M. Merrihue, R. O. Pepin, J. H. Reynolds, *Geochim. Cosmochim. Acta*, **26**, 231 (1962).
14. I. N. Tolstikhin and R. K. O'Nions, *Chem. Geol.* **115**, 1 (1994).
15. D. J. Stevenson, *Lunar Planet. Sci.* **16**, 821 (1985).
16. K. A. Goetel, H. H. Eggert, I. F. Silvera, W. C. Moss, *Eos* **69**, 1436 (1988).
17. J. Matsuda *et al.*, *Science* **250**, 788 (1993).
18. A. P. Jephcoat *et al.*, *Phys. Rev. Lett.* **59**, 2670 (1987).

19. Mao-Bell diamond cells [H. K. Mao, P. M. Bell, K. J. Dunn, R. M. Chrenko, R. C. Devries, *Rev. Sci. Instrum.* **50**, 1002 (1979)] were used with either Re or spring-steel gaskets to compress the samples, which consisted of cryogenically loaded Xe along with Fe powder (<20 μm grain size) and less than 10 volume % fine-grained ruby (<5 μm grain size); the latter is used for pressure calibration [H. K. Mao, P. M. Bell, J. W. Shaner, J. Steinberg, *J. Appl. Phys.* **49**, 3276 (1978)]. Samples were heated inside the diamond cell by means of a Quantronix 117 continuous-wave Nd:YAG laser operated in the TEM_{00} mode, with average temperatures ranging from 1860 (±180) to 3080 (±300) K being documented by imaging spectroradiometry [R. Jeanloz and A. Kavner, *Philos. Trans. R. Soc. London Ser. A* **354**, 1279 (1996)].
20. Diffraction patterns were obtained at high pressures and room temperature (before and after laser heating) using a Rigaku 12 kW/mm^2 rotating anode source of monochromatized Mo K_α x-rays. The diffraction patterns were collected in angular-dispersive mode with film and analyzed by methods described elsewhere [J. H. Nguyen and R. Jeanloz, *Rev. Sci. Instrum.* **64**, 3456 (1993)].
21. The calculations were carried out for the static lattice, corresponding to zero temperature and no zero-point vibrations, with the electron-ion core interaction represented by norm-conserving separable pseudopotentials and the valence wave functions expanded in plane waves up to an energy cutoff of 80 rydbergs (1.09 keV) [L. Kleinman and D. M. Bylander, *Phys. Rev. Lett.* **48**, 1425 (1982)]. In our calculations, the XeFe is arranged in an hcp structure with the A and B layers consisting of Xe and Fe, respectively (space group $P\bar{6}m2$). We assumed a hexagonal unit cell for both $XeFe_2$ and Xe_2Fe, ABC stacking being obtained with, respectively, two layers of Fe and one of Xe or two of Xe and one of Fe (space group $P\bar{3}m1$). To find the minimum enthalpies, we used a quasi-Newton method to relax the internal coordinates and the unit-cell shapes of all structures for a given pressure [B. G. Pfrommer, M. Côté, S. G. Louie, M. L. Cohen, *J. Comp. Phys.* **131**, 233 (1997)].
22. The ratio of Xe/Fe atomic radii, calculated from the theoretically derived volumes of the unit cells of hcp Xe and hcp Fe at 150 GPa, is 1.288. For comparison, 138 out of 164 experimentally observed Laves phases have a ratio of atomic radii between 1.1 and 1.4 [A. E. Dwight, *Trans. Am. Soc. Met.* **53**, 477 (1960)], showing that Xe and Fe are plausible candidates for forming a Laves phase at pressures above 100 GPa. The space group is $P6_3/mmc$ for the Laves phase.
23. See L. V. Woodcock's [*Nature* **385**, 141 (1997)] recent analysis emphasizing the importance of entropic stabilization of the fcc relative to the hcp structure for hard-sphere systems.
24. A. K. McMahan, *Phys. Rev. B* **33**, 5344 (1986).
25. For example, if we assume identical volumes for the fcc and hcp phases V_0 = 35 cm^3/mol [M. Ross and A. K. McMahan, *Phys. Rev. B* **21**, 1658 (1980)], fitting Birch-Murnaghan equations of state to the experimental data yields K_0 = 5.87 (±0.32) GPa and K_0' = 4.81 (±0.09), and K_0 = 5.62 (±0.62) GPa and K_0' = 4.91 (±0.18) for the bulk modulus (K_0) and pressure derivative (K_0') of the fcc and hcp phases, respectively [F. Birch, *J. Geophys. Res.* **83**, 1257 (1978); the subscript zero indicates zero-pressure conditions and the prime designates a pressure derivative]. In contrast, if we assume identical K_0 and K_0' for the two phases, a least-squares fit to our data gives the volume (V_0) of the hcp phase as being 0.3 (±0.5)% larger than that of the fcc phase. Overall, the values of V_0, K_0, and K_0' for the two phases are within mutual uncertainties and are in close agreement with previous determinations [K. Asaumi, *Phys. Rev. B* **29**, 7026 (1984)].
26. Experimentally, we find evidence for a topotactic relation between the two phases, which suggests a martensitic or "military" type transformation [J. W. Christian, *The Theory of Transformations in Metals and Alloys, Part I* (Pergamon, New York, ed. 2, 1975)]. The (111) peak of the fcc phase and the (002) peak of the hcp phase appear at the same d spacing, which implies identical orientations for the close-packed planes in the two structures [A. F. Schuch, R. L. Mills, D. A. Depatie, *Phys. Rev.* **165**, 1032 (1968)]. A similar geometrical relation explains why three other hcp peaks, (004), (112), and (110), are also coincident with the (222), (311), and (220) fcc peaks. It is possible that the detailed transformation mechanism is sensitive to the presence of even small nonhydrostatic stresses, however, so there is no reason to infer a disagreement between experiment and theory on this point.
27. The hcp and bcc phases of Pb also have similar equations of state, a sluggish transformation between phases and a comparable large pressure range in which both phases coexist [H. K. Mao *et al.*, *Solid State Commun.* **74**, 1027 (1990)].
28. B. J. Alder, W. G. Hoover, D. A. Young, *J. Chem. Phys.* **49**, 3688 (1968).
29. P. Loubeyre, *Phys. Rev. B* **37**, 5432 (1988).
30. B. Ruhemann and F. Simon, *Z. Physik. Chem. B* **15**, 389 (1931).
31. Supported by NASA, NSF, and the U.S. Department of Energy (DOE), including grants NSF DMR-9520554 and DOE DE-AC03-76SF00098. The computations were performed on the National Energy Research Scientific Computing Center T3E at Lawrence Berkeley National Laboratory. We thank M. S. T. Bukowinski, R. J. Hemley, M. L. Klein, and R. O. Pepin for helpful discussions.

26 March 1997; accepted 18 June 1997

The World's Smallest Gas Cylinders?

G. E. Gadd,* M. Blackford, S. Moricca, N. Webb, P. J. Evans, A. M. Smith, G. Jacobsen, S. Leung, A. Day, Q. Hua

Argon gas was trapped at high pressure within hollow carbon tubes grown in vapor that have an outer diameter of between 20 and 150 nanometers. The gas was forced into the tubes by hot isostatically pressing (HIPing) the carbon material for 48 hours at 650°C under an argon pressure of 170 megapascals. Energy dispersive x-ray spectroscopy maps and line scans across the tubes show that the argon is trapped inside the bore and not in the tube walls. The room temperature argon pressure in these tubes was estimated to be about 60 megapascals, which indicates that equilibrium pressure was attained within the tubes at the HIPing temperature. These findings demonstrate the potential for storing gases in such carbon structures.

Currently, there is considerable interest in both C fibers (*1–3*) and nanotubes (*4–6*). Apart from efforts to understand the formation process (*7*), attention has been focused on the encapsulation of elements and compounds, particularly oxides and carbides, inside the tubes, as well as within C nanoparticles (*8–11*). On the other hand, the encapsulation of gases such as Ar, Kr, or Xe inside C entities like these has received little attention in the literature, although the trapping of ^{133}Xe may improve its uses in medical imaging such as in the case of the lymphatic system (*12*), where it would be extremely useful to confine the gas physically in some way before injection. Here, we show conclusively how large amounts of Ar can be trapped inside catalytically grown C fibers consisting of multiwalled hollow C tubes with outer and inner diameters ranging from 20 to 150 nm and 10 to 60 nm, respectively.

Hollow C tubes were prepared by catalytic reduction of CO_2 with a modified Vogel process (*13*). In this method, CO_2 was reacted with Zn to produce CO and ZnO, and the CO was subsequently converted on an Fe catalyst to filamentous graphite (*14*). One milligram of finely divided Fe catalyst was placed in the end of a closed quartz reaction tube that had previously had a "Zn mirror" deposited on its inner surface. The reaction tube was placed inside a horizontal tube furnace to maintain the Fe catalyst at 600°C and the Zn mirror at 400°C, and the pressure was monitored to determine when the reaction had gone to completion. An Fe carbide bead crystal formed on the catalyst surface, from which the filamentous graphite "grew."

Scanning electron microscopy of the C produced from catalyzed CO_2 decomposition showed it to be composed of many long and winding C fibers with outer diameters of about 20 to 150 nm, which were interwoven and cemented with large pieces of dense material derived from the catalysts. These features are very similar to those observed by other authors (*15–21*). Backscattered electron imaging indicated that metal was dispersed throughout the fibers and demonstrated that encapsulation had also taken place in the growth mechanism. To investigate the encapsulation of Ar into the various C forms produced catalytically, we hot isostatically pressed (HIPed) the whole sample without any further treatment at 650°C and 170 MPa of Ar for 48 hours. At the end of the HIPing cycle, the gas pressure was reduced from 170 MPa to atmospheric pressure but

Australian Nuclear Science and Technology Organisation, Private Mail Bag 1, Menai, NSW 2234, Australia.
*To whom correspondence should be addressed.